Lithuanian Journal of Physics, Vol. 51. No. 3, pp. 177–193 (2011)

Review

ULTRAVIOLET LIGHT EMITTING DIODES

G. Tamulaitis

Semiconductor Physics Department and Institute of Applied Research, Vilnius University, Saulėtekio 9 – III, LT-10222 Vilnius, Lithuania

E-mail: gintautas.tamulaitis@ff.vu.lt

Received 9 September 2011; accepted 21 September 2011

The paper presents a review of the recent development of III-nitride based deep UV light emitting diodes (LEDs). Main applications of the deep UV LEDs are introduced. Review of material issues is focused on the lattice mismatch between the substrate and the active layer and at heterojunctions in multiple quantum well structures forming the active layer, the localization of nonequilibrium carriers, the material properties limiting the internal quantum efficiency, and the effect of efficiency droop at high density of nonequilibrium carriers. AlGaN is currently the semiconductor of choice for development of deep UV LEDs, so this material is the most discussed one in this review, though some information on AlInGaN is also provided.

Keywords: light emitting diodes, ultraviolet light sources, III-nitride semiconductors, AlGaN

PACS: 42.72.Bj, 78.55.Cr, 78.67.De, 85.60.Jb

1. Introduction

After successful development of blue and white light emitting diodes (LEDs), which are based on InGaN/GaN structures, considerable attempts are being exercised to develop LEDs emitting in ultraviolet (UV) region. The long-wavelength part of the UV radiation ranging in total from 400 nm to 10 nm is traditionally subdivided into three regions: the long-wavelengths range UV-A (400–320 nm), the mid-wavelengths range UV-B (320–290 nm), and the short-wavelengths range UV-C (290–200 nm). To achieve shorter emission wavelengths, wide-band-gap AlGaN, AlInGaN or InAlN compounds are used. The development of UV LEDs proceeds slightly in a shadow of the development of InGaN-based blue, green and white LEDs, which have already huge markets. However, many problems in growth of InGaN and wide-band-gap III-nitrides are similar, so that knowledge and experience gained in study and technology of InGaN is being productively transferred to the development of UV LEDs. Shift of the emission wavelength deeper into UV requires ternary or quaternary III-nitride compounds with larger band gap, which is achieved by incorporation of aluminium. This, however, causes significant problems with structural quality, doping and contacts, and results in a drastic decrease of external quantum efficiency and, consequently, output power when the emission wavelength of an LED is decreased. An example of this feature is illustrated in Fig. 1. Dozens of research groups worldwide are active in development of UV LEDs, and many start-up companies are established to transfer the research results into real devices. LEDs emitting in UV-A region are produced on industrial scale by several companies, however, UV-B LEDs are currently offered commercially only by Sensor Electronic Technology, Inc., based in South Carolina. A considerable impact to the field will definitely be provided by the programme Compact Mid-Ultraviolet Technology (CMUVT), which is recently launched by US Defense Advanced Research Projects Agency (DARPA) and is targeted at development of LEDs emitting at 250–275 nm with an output of 100 mW with 20% wall-plug efficiency and lasers producing 10 mW between 220 and 250 nm without nonlinear frequency conversion.

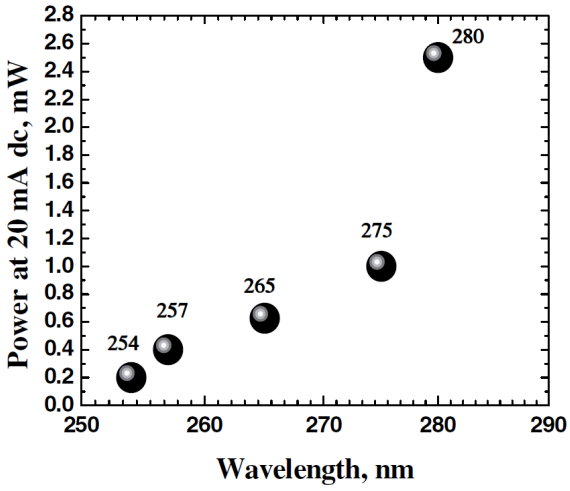

Fig. 1. Output power at 20 mA CW driving current of AlGaN-based LEDs emitting in the range from 280 to 254 nm. After [1].

AlGaN-based structures containing multiple quantum wells (MQWs) are currently the most popular active layers for deep UV LEDs. The energy of the photon emitted by LED is influenced by quantum confinement, strain, and carrier localization in the quantum well but is close to the effective band gap of the material used for the active layer. Though the lattice constant dependence on Al content x in $Al_xGa_{1-x}N$ obeys the linear Vegard's law, the composition dependence of $Al_xGa_{1-x}N$ band gap is nonlinear and can be approximated by expression

$$E_g(x) = (1-x)E_g(\mathrm{GaN}) + xE_g(\mathrm{AlN}) - bx(1-x), \qquad (1)$$

where E_g(GaN) and E_g(AlN) are the band gaps of GaN and AlN, which, at room temperature, are equal to 3.42 eV and 6.13 eV, respectively, and b is the bowing parameter. Quite a few attempts to experimentally evaluate the bowing parameter are reported. For AlGaN, data of 20 references on b are analyzed in the review by Lee *et al.* [2], where the reported b values are grouped mainly in four groups with b in the vicinity of typical values of –0.8, +0.53, +1.3, and +2.6 eV, respectively. This discrepancy can be explained by strain in the epilayers, which strongly depends on substrate and buffer layer used, growth conditions, layer thickness, chemical ordering of the alloy [3–6], cracking of the layer [7] *etc.*

Polarization of AlGaN luminescence has been pointed out as an important feature for optical transitions of AlGaN [8]. Wurtzite-type AlN is a unique wurtzite semiconductor compound having a negative crystal field splitting, as predicted by Suzuki *et al.* [9] and Wei and Zunger [10]. The symmetry of the top valence sub-band in AlN is different from that in GaN (see two side sketches in Fig. 2). Thus, the light emitted due to optical transitions from conduction band to the top valence sub-band in AlN is polarized parallel to the **c** axis of the crystal, while the corresponding emission in GaN is polarized perpendicular to **c**. As a consequence, polarization of $Al_xGa_{1-x}N$ luminescence changes from $\mathbf{E} \perp \mathbf{c}$ to $\mathbf{E} \parallel \mathbf{c}$ with x increasing from 0 to 1 (see Fig. 2) [11]. There the polarization degree is, as usually, defined through intensities of integrated PL components $\mathbf{E} \perp \mathbf{c}$ ($I_\parallel$) and $\mathbf{E} \parallel \mathbf{c}$ ($I_\perp$) as $P = (I_\perp - I_\parallel) / (I_\perp + I_\parallel)$.

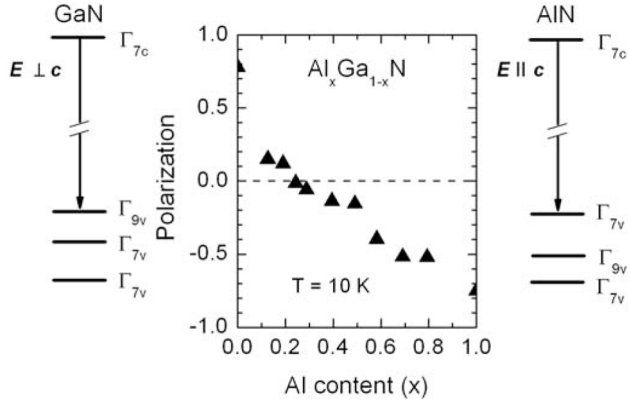

Fig. 2. Luminescence polarization degree measured in $Al_xGa_{1-x}N$ with different aluminium content x and configuration of conduction and valence bands with symmetries of sub-bands and polarization of optical transitions indicated. After [11].

Polarization of the AlGaN emission strongly influences escape of the emission from the epilayers, which are usually grown in **c** direction. This feature is of crucial importance for III-nitride based light emitters, especially for those with high-Al-content AlGaN. Polarization of emission from AlGaN quantum wells is also affected by strain and internal electric field in the structure [12].

Some aspects of the recent development of UV LEDs are already summarized in a few review papers [13–15]. This paper is aimed at the review of the main applications of UV LEDs and the currently key problems in development of wide-band-gap III-nitride materials and structures for these UV emitters.

2. Applications of III-nitride-based UV LEDs

Compared with conventional UV light sources, UV LEDs have obvious advantages of being compact, robust, energy efficient. They also have very bright prospect in increasing their output power, lifetime and in decreasing their price. Some fields of UV

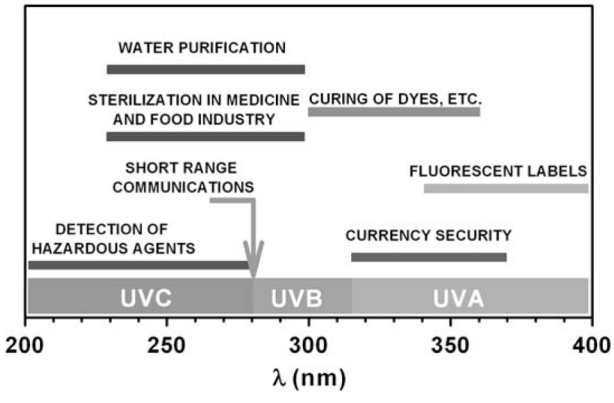

Fig. 3. Wavelength ranges of interest for various UV LED applications.

LED applications are sketched on the wavelength scale in Fig. 3.

Currently the biggest market for UV light sources is water disinfection. There are three methods of water disinfection: chlorination, ozonization, and UV treatment. Chlorination is introduced on a wide scale since 1908. Ozonization produces no taste and odor in the treated water but is still used at a considerably smaller extend than chlorination. UV water treatment is considered more ecologically friendly than chlorine treatment, and its use is expanding. For example, the Catskill and Delaware Ultraviolet Light Disinfection Facility in Mount Pleasant, N. Y., which is planned to be completed in 2012, will treat 2 billion gallons of water per day (still using conventional UV lamps) and supply over 90% of New York City's drinking water [16].

Clean water is the key issue in many developing countries. According to a 2007 World Health Organization report, 1.1 billion people worldwide have currently to drink water of definitely insufficient quality, and more than 1.5 million people die annually from diarrheal diseases caused by contaminated water. However, not the developing countries but rather the military, as it is often the case for emerging technologies, is currently the driving force in developing UV LED based systems for water purification. Up to now, the military used bulky, truck trailer size devices containing fragile mercury lamps and equipped with powerful power supplies to decontaminate water for soldiers in contaminated terrains. A personal cup with a UV LED decontaminating the water inside the cup within a minute or even a shorter period of exposition just before using it can solve the water purification problems in a considerably more convenient and efficient way.

Traditionally, emission of mercury lamps at 253.7 nm is used for water disinfection. Meanwhile, the output power of currently available UV LEDs is already sufficient for disinfection of both bacteria and viruses. Disinfection of viruses usually requires a higher UV dosage than that for bacteria. Selection of optimal wavelength is also important for disinfection efficiency.

UV LED treatment can be also used for decontamination of various surfaces as well as for disinfection in food industry and medicine. An ultraviolet germicidal mask to disinfect air for personal use is patented in 1992, well before the development of UV LEDs [17]. Application of LEDs makes such a device really portable and effective.

The combination of the deep UV LED based decontamination equipment with contamination detection systems enables an automated feedback to ensure reduction and maintenance of contamination level below a specified value [18, 19].

The development of computers raised importance of information storage. As a response to this urgent need, an ancient technique to store information by making cuneiform pits in a clay tablet was revived. Application of a binary system operating with two digits 0 and 1 substantially simplified the recording, the use of laser diodes enabled a significant increase in information storage density, and the current progress in materials science provided superior substitutes for clay in production

of optical storage discs. Shorter light wavelengths enables light beam into a smaller spot, since the spot size is limited by self-diffraction. For decades, this feature was important for storing information on optical disc media. Due to availability of reliable laser diodes, the 780 nm wavelength emission of GaAs / AlGaAs laser diodes (LDs) was set as a standard for CDs, 650 nm emission delivered by LDs based on the same GaAs / AlGaAs materials system was the wavelength set for DVDs, while switching to InGaN-based LDs enabled reduction of the wavelength down to 405 nm, both for Blu-ray and HD-DVD recording formats. A few years ago, the further decrease of the wavelength in setting new optical disc formats has been pointed out as one of the driving forces for development of UV solid-state light emitters. However, the recent bursting progress in the development of flash memory and Internet services will result in substantially new techniques of distributing audio and visual information and will, probably, leave the optical discs beside the mainstream of information technologies.

UV LEDs might be used in specific short-range communication technologies. One of the targets in the SUVOS program, which is completed by the US Defense Advanced Research Projects Agency (DARPA) a few years ago, was developing a UV-based transceiver for covert non-line-of-sight (NLOS) optical communications. The deep UV light is efficiently absorbed in the air and, consequently, prevents interception of the communication signal by enemy located at a distance from the squad using the NLOS system. In the NLOS system, a small fraction of the modulated UV light at 280 nm, which is emitted by an LED-based transmitter, is scattered by molecules and aerosols in the air to be detected at a distance of up to ~250 m. The signal outside this range is too weak to be detected [20]. Solar-blind detectors for these systems are also fabricated using AlGaN epilayers. The band gap of this compound is tailored to be too wide to absorb the visible light, but effective in absorption at 280 nm. Since the atmosphere effectively absorbs radiation at 280 nm, the background level in this spectral range is weak.

UV LED is a prospective light source for excitation in spectroscopic studies. Application of LEDs considerably decreases the size, weight, and energy consumption of spectroscopic systems and enables fabrication of portable, robust and autonomous devices for detection of hazardous chemical and biological agents. Such devices can be used for monitoring the hazardous agent concentration or detection of sudden release of the agents in terrorist attacks.

LED is a very convenient light source for modulation spectroscopy. The output power of a UV LED can easily be modulated up to the frequency of 300 MHz by modulation of the driving current. This feature is being successfully exploited in frequency domain fluorescence lifetime (FDFL) measurements, which have been developed to follow excitation dynamics in various systems many decades ago, even before introduction of time-resolved laser spectroscopy. In FDFL measurement technique, the sample is excited by the light of modulated intensity. The photoluminescence response is, consequently, also modulated, however, with certain phase shift and a changed modulation depth. The measured frequency dependence of the latter two parameters is used to extract the photoluminescence time evolution by using a Fourier-transform analysis [21]. This technique enables extraction of fluorescence decay times at very low excitation power densities in a very broad range from miliseconds down to subnanoseconds.

In detection of hazardous agents, capability to extract fluorescence lifetimes is a valuable supplement for fluorescence spectroscopy, since the emission spectra of the agents to be detected are usually broad and overlap. Application of LEDs with a broad choice of emission wavelength offers attractive opportunities for selective excitation. All these features can be utilized in a compact, robust, low-energy-consumption portable device for *in site* detection of hazardous chemical and biological agents. Prospects of application of such device to detect spores of *Bacillus anthracis*, which are the pathogen of the Anthrax disease, have been demonstrated on the spores of *Bacillus globigii*, which are model spores for *Bacillus anthracis* [22]. Combination of FDFL measurements with spectroscopy at selective excitation enabled revealing a specific area for *Bacillus globigii* on the plot presented in Fig. 4. The FDFL measurements have also been successfully applied in detection of the basic biological autofluorophores (nicotinamide adenine dinucliotide, riboflavin, tyrosine, and tryptophan) [23].

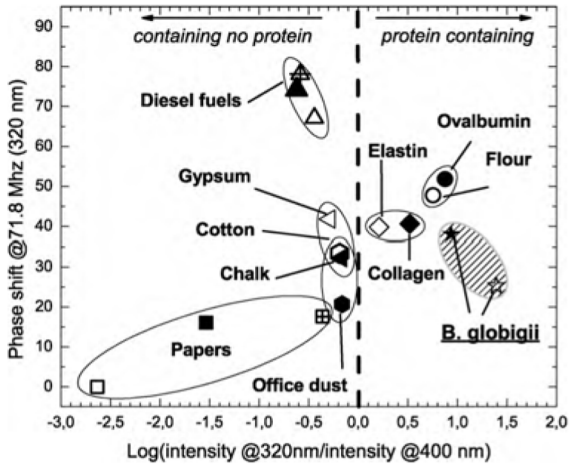

Fig. 4. Plot of the fluorescence phase shift at 70 MHz in the 320-nm spectral window versus 320-nm to 400-nm fluorescence intensity ratio for *B. globigii* spores and of common airborne interferants. Plot area specific for *B. globigii* spores is highlighted. Reprinted from [22] with permission.

LEDs emitting in UV-A region have higher output powers and longer lifetimes than deep UV LEDs and already found many applications on an industrial scale.

In accordance with the absorption spectrum of materials used for dental filling, mainly the emission at ~370 nm is currently used for UV curing in odontology. LED-based curing devices have obvious advantages against the corresponding devices based on xenon discharge or halogen lamps. They need no bulky power supplies, no filters to select the necessary wavelength, no cooling. Due to these advantages, the UV LEDs already became the light source of choice in the dental curing lamps currently on sale. UV LEDs emitting in the range 300–365 nm are also used for curing various polymers, printer inks, adhesives, varnishes, and coatings in many applications.

"Black light" at ~370 nm lures mosquitoes, flies (flies are most attracted to the light at 365 nm [24]), and other insects and is used in bug zapper, where the insects are electrocuted providing chemical-free bug protection. Bug zappers equipped with UV LEDs consume considerably less energy and are more compact and robust than those containing conventional lamps with Wood's glass. A small solar panel might be sufficient to supply energy for the LED bug zappers.

LEDs emitting in UV-B region are used in medicine for phototherapy and photochemotherapy. Wavelengths of 311–313 nm are most effective for phototherapy of psoriasis [25]. LEDs can also be used for healing vitiligo, eczema and other skin deceases.

To help prevent counterfeiters, banknotes and sensitive documents like credit and ID cards, passports, and driver's licenses usually contain watermarks or fibers visible only under UV illumination. Compact LED-based UV light sources are often much more convenient in use for checking the watermarks than the UV fluorescence lamp based devices, which are predominantly in use up to now. UV LED lamps are also useful in forensics, identification of rocks and minerals in field conditions, and other applications.

In spite of significant achievements, deep UV LEDs are still a disruptive technology providing essentially new features like compactness, low energy consumption, easy output modulation. Consequently, several completely novel applications for these UV sources might emerge in the future. For example, it is recently shown that supplemental UV-B radiation increases the content of phenolic compounds in plants and helps to preserve them during storage after harvest [26]. Improvement of UV LEDs might make this technology cost-effective.

3. Problems and achievements in developing structures for UV LEDs

3. 1. Lattice mismatch

Many problems encountered in developing devices based on III-nitrides in general and on AlGaN in particular are related with lattice mismatch, both between the substrate and the subsequent epilayer [27] and between the adjacent layers of different composition in heterostructures. Techniques for growing AlN monocrystals to be used as substrate material for epitaxy of high-Al-content AlGaN with low lattice mismatch are difficult, expensive and still produce monocrystals much smaller than those desired for commercial growth of III-nitride based devices. Though approximately four decades passed since the first successful attempts of growing bulk AlN crystals [28–30], only the efforts resumed a decade ago lead to a substantial progress in the

production of larger AlN single crystals exceeding 1 cm in length and 0.5 cm in diameter and having a dislocation density of less than 10^4 cm^{-2} [31]. These crystals have been successfully used as substrates to deposit $Al_{0.5}Ga_{0.5}N$ epilayers of high structural quality [32, 33]. Their high crystal quality was confirmed by observation of stimulated emission at then record-short wavelength of 258 nm [34]. Attempts for commercialization of LEDs based on low-dislocation-density AlN substrates are being exercised by company Crystal IS, Green Island, NY. Recently, quite high output power of 9.2 mW at 260 nm has been reported for LEDs fabricated on bulk AlN [35]. However, this approach is still not widespread, probably, due to high price and very limited availability of bulk AlN substrates.

During the last decade, hydride vapor phase epitaxy (HVPE) proved to be a very prospective technique to grow high-quality, thick, bulk-like AlN layers. Highly stable deep UV LEDs emitting at the wavelength of 285 nm were fabricated by deposition via pulsed atomic layer epitaxy over a 15-μm-thick AlN-sapphire template which was prepared by metalorganic hydride vapor phase epitaxy [36].

The lack of native substrates excluded the III-nitride materials from the list of prospective wide-band-gap semiconductors for a long period of time since the first GaN crystals were synthesized in 1940 [37] and the first large area layers of GaN on sapphire were grown by Maruska and Tietjen using a chemical vapor deposition technique in 1969 [38]. The quality of the epilayers was drastically improved by growing a low-temperature-deposited buffer layer of AlN [39] or GaN [40] between the substrate and the high-temperature GaN layer. This improvement performed by research group headed by Prof. I. Akasaki at Nagoya University and Dr. S. Nakamura at Japanese company Nichia, Inc., together with discovery of means to activate p-type impurities, gave an impact for tremendous progress in development of blue and white LEDs in the last decade of the XX century and afterwards. The buffer layer serves for nucleation of defect-free areas and decreases the dislocation density in the subsequent epilayer grown at higher temperature. Improvement of the buffer layer is still one of the key issues in the search of means to improve performance of III-nitride heteroepilayers. Most of these attempts are directed to improve performance of InGaN-based LEDs, which already have a tremendous industrial importance. A lot of experience gained in these attempts is transferred to development of buffer layers for AlGaN-based LED structures.

Calculations show that the strain can be significantly reduced by superlattice buffers [41, 42]. This approach is successfully applied for growing AlGaN-based structures [14].

As it is demonstrated for the first time for GaN epilayers more than a decade ago [43, 44], the density of threading dislocations can be diminished by orders of magnitude by applying epitaxial lateral overgrowth (ELOG) approach. In ELOG, growth of the epilayer is interrupted, surface at certain periodically closely spaced areas of the layer (usually stripes) are modified to inhibit the subsequent deposition (e. g., by growth of SiO_2 or mechanical damage of the surface). The subsequent growth starts only above the unmodified areas but spreads laterally over the modified areas. Dislocations develop predominantly in the main, transverse growth direction, while their density in the wing areas is lower by several orders of magnitude. The growth usually is carried out until the full coalescence of the wings. Combination of MEMOCVD® approach with the ELOG method to accomplish migration-enhanced lateral overgrowth (MELEO) of AlN and AlGaN has been proven to be efficient to improve the performance of UV LEDs [45].

The development of high Al content AlGaN heterostructures is strongly impeded by a considerable lattice mismatch at heterointerfaces. The large lattice mismatch in AlGaN / GaN or AlGaN / AlGaN heterostructures decreases the critical thickness of a fully strained AlGaN barrier and results in uncontrolled local strain relaxation at the heterointerface via generation of misfit dislocations and cracks.

The lattice matching can be achieved by using quaternary compound AlInGaN. Incorporation of Al increases the band gap and decreases the lattice constant, while incorporation of indium has an opposite effect. As can be seen in Fig. 5a, incorporation of Al and In at a ratio of 5 to 1 results in lattice matching of such quaternary AlInGaN and GaN. Meanwhile the band offset between these two materials at the Al/In ratio of 5 : 1 is still sufficient to form a quantum well.

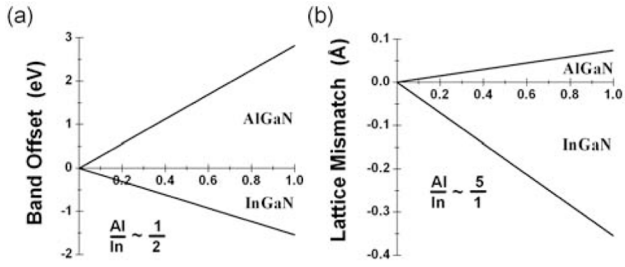

Fig. 5. Dependence of lattice mismatch and band offset on Al and In content x in ternary compounds $Al_xGa_{1-x}N$ and $In_xGa_{1-x}N$.

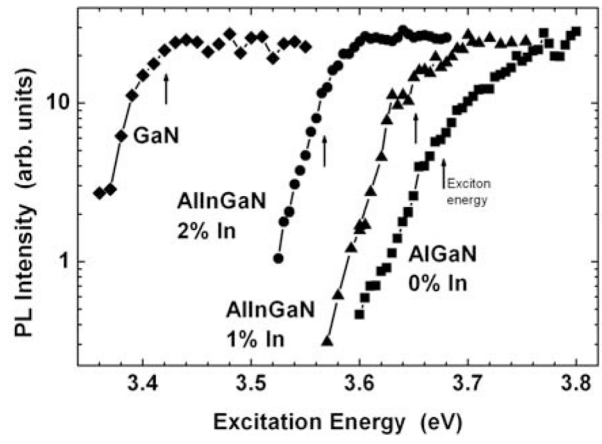

Fig. 6. Dependence of spectrally integrated luminescence intensity on incident photon energy in AlInGaN with 0, 1%, and 2% of In, and GaN buffer layer. Arrows indicate exciton energies. After [50].

After the first successful growth of AlInGaN epilayers on sapphire substrate [46], application of this quaternary compound has been considered as an attractive approach for improving the structural quality of wide-band-gap nitride heterostructures [47]. The independent lattice matching and band gap engineering can also be used to control piezoelectric doping [48, 49], i. e., the formation of 2D electron gas under the influence of the piezoelectric field built in at the heterointerface [41].

The quality of AlInGaN layers with Al mole fractions in excess of 40% was significantly improved by application of the pulsed atomic layer epitaxy (PALE) technique, and strong enhancement of room-temperature photoluminescence peaking at 280 nm was achieved [50]. The PALE approach allows for accurate control of the quaternary layer composition and thickness by changing the number of aluminum, indium, and gallium precursor pulses in a unit cell and the number of unit cell repeats. This technique enables growth of the quaternary AlInGaN layers even at temperatures lower than 800 °C.

Using reflectivity, site-selectively excited photoluminescence, photoluminescence excitation, and time-resolved luminescence techniques, it is demonstrated that the incorporation of In into AlGaN layers results in a significant improvement of the material quality and optical properties of the quaternary AlInGaN alloy [51]. Figure 6 depicts the dependence of the spectrally integrated luminescence intensity on the incident photon energy in AlGaN, AlInGaN with approximately 1 and 2% In content, and GaN buffer layer. It is evident that the most abrupt band gap is formed in AlInGaN with approximately 2% of indium, which corresponds to a nearly lattice-matched growth of $Al_{0.09}In_yGa_{0.91-y}N$ on GaN.

Unfortunately, essentially different optimal temperatures needs for the growth of ternary compounds InGaN and AlGaN substantially impede selection of growth temperature for quaternary AlInGaN compound, especially in wide-band-gap AlInGaN with high Al content. Thus, most of research groups previously active in development of AlInGaN-based structures abandoned these attempts and switched to optimization of AlGaN-based wide-band-gap structures. Significant progress in growth technologies, e. g. migration-enhanced metal-organic chemical vapor deposition MEMOCVD® technique [52, 53], and innovative design involving narrow quantum wells to avoid the influence of built-in electric field [54] and the phonon engineering approach [55] enabled a significant increase in the output power of deep UV LEDs. The cw output power of a single chip UV LED emitting at 280 nm has been reported to surpass 10 mW a few years ago [56, 57].

3.2. Quantum confined Stark effect

Due to different material polarity of the adjacent layers in AlGaN / AlGaN or AlGaN / AlN heterostructures, a spontaneous polarization occurs at the interface. Moreover, these materials are piezoelectric. Thus, the strain due to lattice mismatch at the interface induces a piezoelectric polarization. The polarizations induce built-in field, and the quantum

well transforms into a triangle shape, as sketched in Fig. 7. As a result, the effective band gap (distance between the lowest energy levels for electrons and holes) decreases (the PL band shifts to the long wavelength side), and the probability of radiative recombination decreases due to decreased overlap of the electron and hole wavefunctions. This effect is called the quantum confined Stark effect (QCSE) by analogy with the conventional Stark effect manifesting in shifting and splitting of the spectral lines of atoms and molecules that are caused by an external static electric field.

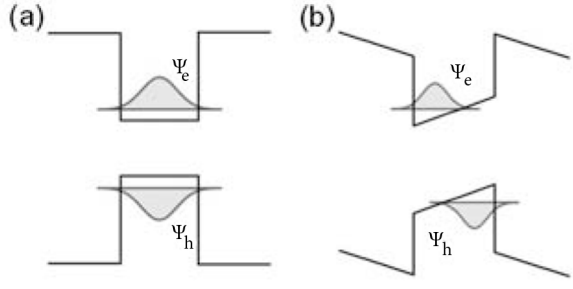

Fig. 7. Electron and hole wave function in a quantum well without (a) and with (b) built-in quantum well.

The value of the built-in field can be calculated using material parameters [58]. However, some of these parameters are measured indirectly or with insufficient accuracy. The inaccuracy in material parameters might be claimed to be responsible for discrepancy between theory and experiment: the field experimentally estimated in AlGaN heterostructures is smaller than the corresponding calculated values [59, 60].

The built-in field might be screened by nonequilibrium carriers. The screening results in emission enhancement due to better overlap of electron and hole wavefunctions and in a blue shift of the PL band due to transformation of the quantum well from triangular to rectangular shape [61, 62]. This behavior can be simulated by simultaneously solving the stationary Schrödinger equation and the Poisson equation describing the asymmetric space–charge distribution in the well.

The blue shift caused by the screening is difficult to distinguish from that caused by filling-in of the localized states [63, 64]. In InGaN alloy, the contributions were revealed by comparing the PL dynamics at increasing excitation power densities in bulk epilayers and InGaN / GaN MQWs. The blue shift observed with increasing excitation intensity in bulk materials is caused by filling of band-tail states, while the blue shift in MQWs is caused initially by the screening of the internal electric field and, later on, by filling of band-tail states [65]. A similar effect has been observed in UV photoluminescence dynamics of highly excited quaternary AlInGaN epilayers and MQWs [66].

The internal built-in field can be avoided by growing AlGaN epilayers and heterostructures in nonpolar or semipolar directions. The internal-field-free quantum structures grown on *R*-plane sapphire might be promising for fabrication of UV LED due to higher emission intensity and stable spectral parameters [67]. A semipolar AlGaN-based UV LED emitting at 307 nm was recently grown on an m-plane sapphire substrate [68].

Another successful approach to diminish the influence of the QCSE is the reduction of the well width in the active MQW layer until the QCSE becomes insignificant [54].

3.3. Carrier localization

Fluctuations of InGaN alloy composition, i.e. formation of In-rich regions, have been predicted in thermodynamic calculations and observed in spatially resolved cathodoluminescence [69], near field optical microscopy [68], high resolution transmission electron microscopy, and X-ray diffraction microanalysis [71, 72] experiments. The effect becomes stronger with increasing the average In content, especially above 20% of In, and inhibits development of LEDs in green and longer wavelengths range. Even small composition fluctuations result in localization of nonequilibrium carriers in regions with lower potential due to a locally higher In content. According to thermodynamic calculations, AlGaN alloys do not have unstable mixing regions and no phase separation was expected in AlGaN epilayers [73]. For some time, AlGaN compounds have been considered to be homogeneous. However, further investigations evidenced considerable carrier localization also in AlGaN epilayers and heterostructures.

The carrier localization is usually evidenced by a specific temperature dependence of photoluminescence band parameters. The peak position of the

band due to band-to-band recombination in semiconductors usually follows the continuous band gap shrinkage with increasing temperature as it is phenomenologically described by the Varshni formula [74] or a Bose-Einstein-like formula with adjustable parameters for every material. In semiconductors with considerable carrier localization, the temperature dependence of the PL band peak position shows an abnormal S-shape. The initial red shift in the S-shaped dependence reflects the thermally enhanced ability of the localized excitons to reach the lowest available energy sites via hopping [75–77]. The further temperature increase results in thermalization of the exciton system, in a high-energy shift of the exciton distribution, and, consequently, in a blue shift of the PL band position [76]. At elevated temperatures, this blue shift is overwhelmed by the band gap shrinkage, and the band experiences a red shift again. The same processes cause also a W-shaped temperature dependence of the band width. Thus, the S-shape and W-shape of the PL band peak position and width, respectively, can be treated as a fingerprint of exciton localization.

The S-shaped temperature dependence of the PL peak position was observed in ternary AlGaN [78–80] grown at certain conditions, as well as in quaternary AlInGaN [81–83], thus, indicating exciton localization in these alloys. The S-shape in the peak position dynamics is usually accompanied by strong spectral dependence of PL decay time [81, 84]. This dependence is consistent with the model of localized excitons: the lower is the energy of a localized exciton, the lower is the probability for hopping of this exciton to a center of nonradiative recombination. Thus, the excitons emitting photons of lower energy have a longer lifetime. The abnormal temperature dependence of the PL peak position is observed in $Al_xGa_{1-x}N$ in a wide range of x up to 0.7 [84]. The S-shape and W-shape temperature dependences of the band position and width in AlGaN and AlInGaN are presented in Fig. 8.

As illustrated in Fig. 9, the S-shape and W-shape temperature dependences of band position and width are observed only at low carrier densities. At elevated carrier densities, all localized states are occupied, and the dependences have a monotonous shape.

In AlGaN QWs, the potential fluctuations leading to carrier localization can be also caused by fluctuations in the width of the QWs.

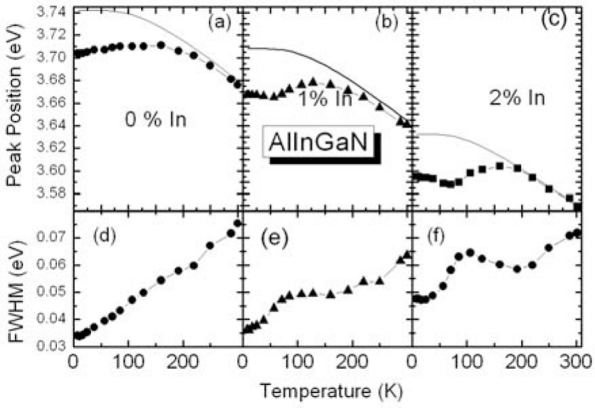

Fig. 8. Temperature dependence of luminescence peak position (points in (a) to (c)), exciton energy (solid lines in (a) to (c)), and full width at half maximum (points in (d) to (f)) for AlGaN and AlInGaN with 1% (b) and (e), and 2% (c) and (f) of In. Reprinted from [83] with permission.

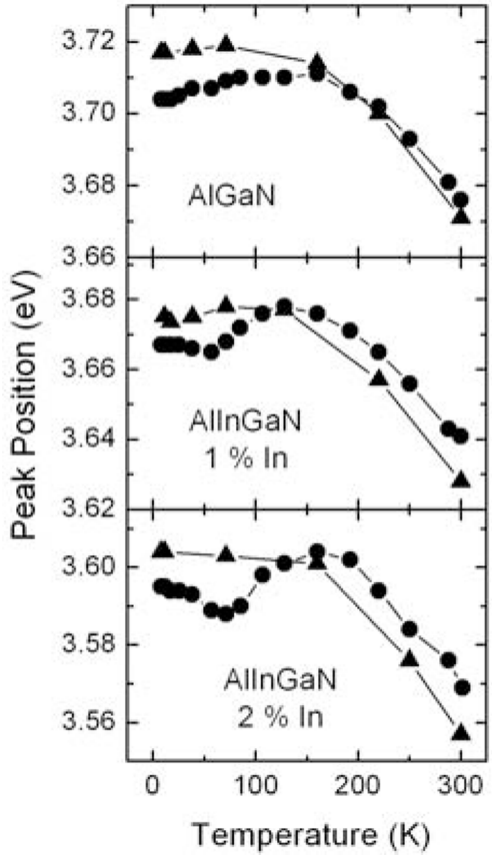

Fig. 9. Temperature dependence of the peak position of the luminescence band under 7 kW/cm^2 (dots) and 910 kW/cm^2 (triangles) excitation power densities for AlInGaN samples with different indium content (indicated). After [82].

The simulation of the PL temperature dynamics can be performed using the Monte Carlo simulation procedure developed by Baranovskii *et al.* [85] and Skolnick *et al.* [86]. The rate of phonon-assisted exciton hopping between localized states *i* and *j*, which are distributed randomly in space with the density *N* and are separated by distance r_{ij}, can be defined by Miller-Abrahams expression

$$\nu_{ij} = \nu_0 \exp\left(\frac{2r_{ij}}{\alpha} - \frac{E_j - E_i + |E_j - E_i|}{2k_B T}\right), \quad (2)$$

where E_i and E_j denote the energies of the initial and final states, respectively, ν_0 is the attempt-to-escape frequency, and α specifies the decay length of the exciton wave function. The exciton behavior is simulated by random selection of either hopping to another localized state with the rate calculated using eq. (2) or radiative annihilation from the current state with the rate τ_0^{-1}. The energies of the localized states at which the event of radiative annihilation occurred are recorded to compose the emission spectrum.

The fitting of the simulated temperature dependence of the PL peak position with the experimental results obtained in $Al_{0.1}In_{0.01}Ga_{0.89}N$ [87] is depicted in Fig. 10. Although the simulated temperature dependence of the Stokes shift (i. e. the difference between exciton energy and PL peak position) quantitatively agrees with the experimental one (Fig. 10a), the simulated FWHM is considerably narrower than the measured values (Fig. 10b). To achieve a quantitative description of the temperature dependence of both the Stokes shift and FWHM in the entire temperature range, a model of a double-scaled potential profile has been introduced. The model implies formation of low-potential regions, where excitons at low temperatures move by hopping over chaotic potential fluctuations with a dispersion parameter σ. The average exciton energy in different regions is dispersed with the dispersion parameter Γ. Consequently, the overall emission band is a superposition of the bands due to exciton annihilation in each region. The band shape $S_0(h\nu)$ can be calculated as a convolution

$$S(h\nu) = \int S_0(h\nu')\, G(\Gamma, h\nu - h\nu')\, \mathrm{d}\, h\nu', \quad (3)$$

where $G(\Gamma, h\nu)$ is a standard Gaussian function with dispersion Γ^2.

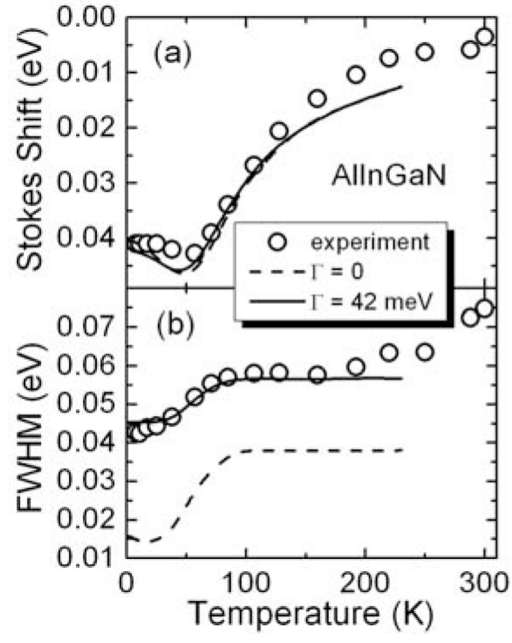

Fig. 10. Temperature dependences of the Stokes shift (a) and FWHM (b) in the $Al_{0.1}In_{0.01}Ga_{0.89}N$ epilayer obtained experimentally (dots), calculated straightforwardly from Monte Carlo simulation for the potential roughness σ = 16 meV (dashed lines), and according to the double-scaled potential profile with an additional broadening Γ = 42 meV (solid lines). Reprinted from [87] with permission.

The double scaled potential profile is sketched in Fig. 11. The model ensures good approximation for the PL band shape, quantitatively describes the temperature dependence of the band FWHM, and enables one to extract absolute values of the dispersion parameters *σ* and Γ. This model is applicable to describe the potential profile in InGaN [88], AlInGaN, [59, 89] and AlGaN [90]. The model of the double-scaled potential profile is also consistent with the recent results obtained by near-field optical spectroscopy of AlGaN epilayers with different Al content [91]. Potential fluctuations on a small spatial scale (<100 nm) were evaluated from the width of the photoluminescence spectra to be between 0 and 51 meV and to increase with increased Al content. These potential variations have been assigned to compositional fluctuations due to stress variations, dislocations, and formation of Al-rich grains during growth. Larger area potential variations of 25–40 meV were more clearly observed

in the lower-Al-content samples and were attributed to formation of Ga-rich regions close to grain boundaries or atomic layer steps. Gallium-rich regions at grain boundaries have been previously observed using cathodoluminescence and explained by a higher compressive strain (that is favorable for incorporation of Al) in the central area of the grains [92] and the larger lateral mobility of Ga adatoms on the growth surface and their accumulation at the grain boundaries [93]. To accommodate the relative difference in crystal orientation among the coalescing grains, the grain boundaries usually contain high density of extended defects [94]. As demonstrated in GaN [95], the extended defects, decorated with point defects, act as nonradiative recombination centers.

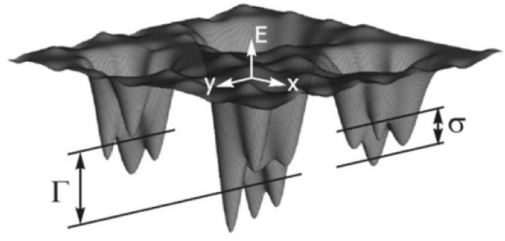

Fig. 11. Schematic plot of a double-scaled potential profile. Dispersion of the distribution of localized states within each low-potential region σ and the dispersion of the distribution in average localization energy in the regions Γ are indicated. After [90].

As mentioned before, the observed dynamics of the PL characteristics with temperature and pump intensity might also be influenced by the built-in electric field, which is partly or completely screened at elevated carrier densities. The PL band dynamics is also influenced by band gap renormalization and carrier heating [96].

3.4. Internal quantum efficiency

The external quantum efficiency of an LED depends on efficiency of three processes: carrier injection into the active region, radiative carrier recombination, and light extraction out of the chip. As a result of the recent progress in improvement of ohmic contacts, enhanced conductivity of n and p layers, and optimized chip configurations, the injection efficiency reaches, probably, up to ~90%. The light extraction efficiency is considerably lower but experienced considerable growth during the last decade for InGaN-based LEDs. In planar configuration, only ~4% of light emitted in the active layer escapes out of the chip crystal, since the angle of the total reflection in semiconductors is small (~20^0), and a large part of light experiences multiple reflections, reabsorption and is lost due to nonradiative recombination. Many chip designs have been suggested to increase the light extraction of LEDs: encapsulation in epoxy dome, thick layers to increase the number of escape cones, Bragg reflectors on the backside of the chip, flip-chip configuration, substrate lift-off, surface roughening etc. AlGaN-based deep UV LED design is still not optimized, so considerable progress is still expected on this issue.

Another field of UV LED efficiency improvement is enhancement of the internal quantum efficiency (IQE) that reflects the ratio of the number of photons emitted in the active region to the number of carriers injected there. The IQE depends on the ratio between radiative and nonradiative recombination rates. Due to a large density of extended and point defects, the nonradiative recombination rate in AlGaN epilayers at room temperature is high and considerably exceeds the radiative recombination rate. The density of nonradiative recombination centers increases with increasing Al content in AlGaN. Localization of carriers (excitons) inhibits their ability to reach the nonradiative recombination centers by hopping through the localized states and to recombine there nonradiatively. Since the hopping and capture of the carriers into the nonradiative recombination centers occurs over potential barriers, a decrease in temperature suppresses the nonradiative recombination.

It is usually assumed that the nonradiative recombination is negligible at temperatures below 10–20 K. This assumption makes the base for the technique that is usually applied to estimate the IQE experimentally. Following Watanabe *et al.* [97] the emission efficiency η_{PL} can be defined, as:

$$\eta_{PL} = C \frac{I_{PL}/h\nu_{PL}}{I_{EX}/h\nu_{EX}}, \tag{4}$$

where I_{EX}, $h\nu_{EX}$ and I_{PL}, $h\nu_{PL}$ are intensities and photon energies for the excitation and emission,

respectively. The constant C depends neither on temperature nor on the pump intensity, provided that the conditions of excitation and signal detection are maintained unchanged during the experiment and $h\nu_{EX}$ considerably exceeds the effective band gap in the structures under study, so that no significant changes in absorption coefficient for the laser light are expected. Consequently, the experimentally observed change in emission intensity should reflect the temperature dependence of IQE. To reach the reference point of 100%, photoluminescence intensity is measured as a function of temperature down to ~10 K.

The assumption that the IQE at low temperatures equals 100% is very convenient but quite often incorrect, especially in materials with high density of nonradiative recombination centers and strong potential fluctuations to cause carrier localization. Nevertheless, the assumption is used because of the lack of any other, more accurate techniques to estimate IQE. Moreover, the dependence of IQE on temperature depends on excitation power density, as shown in Fig. 12.

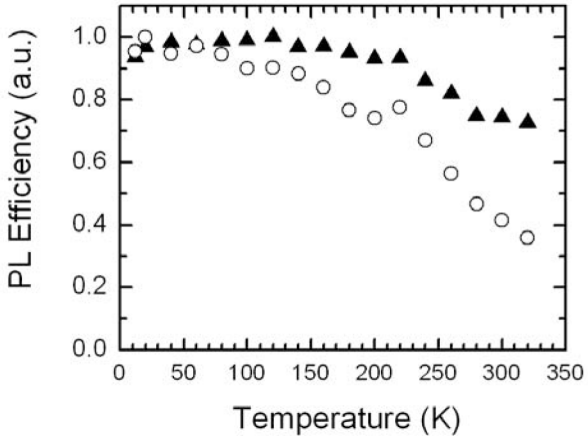

Fig. 12. Temperature dependence of photoluminescence efficiency in $Al_{0.35}Ga_{0.65}N$ multiple quantum well structure at excitation power density of 200 (triangles) and 3 kW/cm^2 (dots).

The IQE of AlGaN epilayers and MQWs is currently considerably increased by optimization of growth temperature, precursors flow rates, and improvement of buffer layers. Higher IQEs are achieved by using pulsed supply of group III and V precursors. Room temperature IQE of 70% is reported at 280 nm in $Al_{0.35}Ga_{0.65}N$ MQWs [98] fabricated by migration-enhanced metal-organic chemical vapor deposition, MEMOCVD®, technique [99, 100]; 69% were estimated at 247 nm in AlGaN / AlN QWs fabricated by modified migration enhanced epitaxy (MMEE) [101]. In general, IQE decreases with increasing Al content. For example, in AlGaN / AlN MQWs, IQE was estimated to be 50% and 5% for the structures emitting at 250 nm and 220 nm, respectively [102]. Note, however, that the absolute IQE values, as discussed above, reflect the upper limit of the real values and might be considerably lower than the values reported.

3.5. Efficiency droop

For many applications, the total light flux delivered by an LED chip is of major importance. The flux might be increased by increasing both the external quantum efficiency (EQE) and the driving current. However, as it was observed first for blue and green InGaN-based LEDs [103–105], the increase of the driving current results in reduction of EQE, and the light output increases sublinearly when the driving current is increased. A term "efficiency droop" or just "droop" was coined for this effect. Unfortunately, the droop unavoidably occurs also in AlGaN-based UV LEDs, as it is illustrated in Fig. 13 for a 245 nm UV LED.

A review of the possible origins of the efficiency droop can be found in [107]. Filling in of the

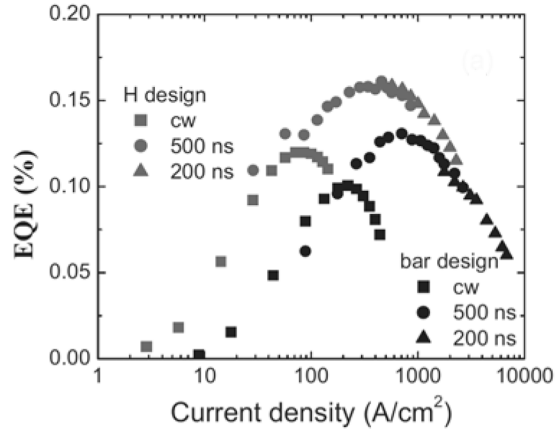

Fig. 13. External quantum efficiency as a function of driving current density for 245 nm LED operating in CW and pulsed modes. Reprinted from [106] with permission.

localized states, carrier recombination outside the MQW active region [108–110], or tunneling out of the wells [111], screening of the localization potential fluctuations, junction heating [112], and thermally assisted current transport along the threading dislocations in III-nitride layers [113] have been proposed to explain the origin of the droop. Recently, a lot of study and discussions has been attracted by suggestion that Auger recombination, i. e. the recombination of electron and hole by transferring their energy to the third interacting quasiparticle (electron or hole), is responsible for the droop [114, 115]. Auger processes are often the dominating recombination process in highly excited narrow-band-gap semiconductors but were considered ineffective in semiconductors with the band gap exceeding approximately 0.6 eV [116], since requirements for energy and momentum conservation cause an exponential decrease of the probability of the Auger processes with increasing band gap. Involvement of intra-band transitions, electron-phonon coupling and alloy scattering significantly increases the rate of Auger recombination in InGaN [117, 118]. There are no calculations or direct experimental estimates for the Auger recombination rate in AlGaN, where the rate should be significantly lower due to a wider band gap. Moreover, as it is evident in Fig. 14, the enhancement due to the resonant transition of the interacting electron to the higher subband, that is important for InGaN with the band gap close to 2.5 eV, is negligible for AlGaN, where the energy gap for the intraband transition has a similar value. The recombination rate in Fig. 14 is, as usually, expressed via the Auger coefficient that is one of the coefficients used in the rate equation for electron density n (it is supposed that the hole and electron densities are equal under high-excitation conditions typical for LEDs in action). The rate equation is often called an ABC model for electron dynamics and contains generation term G and three recombination terms: a linear recombination term with the rate constant A, a bimolecular recombination term with the coefficient of bimolecular recombination B, and an Auger recombination term with Auger coefficient C:

$$\frac{\mathrm{d}n}{\mathrm{d}t} = G - An - Bn^2 - Cn^3. \qquad (5)$$

In spite of intense recent study, the problem of the droop origin still has no unambiguous answer.

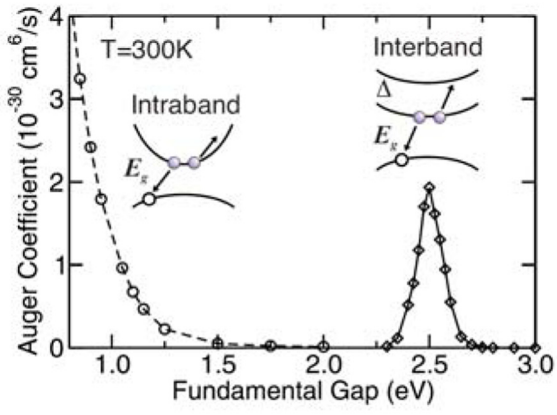

Fig. 14. Auger coefficient for interaction of light hole with two electrons as a function of fundamental band gap for a simulated InGaN alloy. Intraband and interband processes are illustrated in the insets above the regions of their dominance. Reprinted from [117] with permission.

Unfortunately, this is not just a scholarly problem. Understanding the droop origin would help to purposefully change material properties or device design to achieve a higher output power. According to the knowledge accumulated by many research groups, several mechanisms of the droop might simultaneously play an important role. For example, a study of Sun et al. of AlGaN LEDs emitting at 245–247 nm showed that junction heating is important for the droop to occur but is not the single origin of the droop observed [112].

It is worth noting that equation (5) might be an oversimplified model of carrier dynamics in real III-nitride devices at high injection or photoexcitation levels. The model supposes that the rate of recombination at nonradiative recombination centers is proportional to the carrier density. However in III-nitride heterostructures, localization of the part of nonequilibrium carriers might be strong enough to prevent hopping of these carriers (excitons) to the nonradiative recombination centers. Thus, the fraction of the carriers that are able to recombine at nonradiative recombination centers depends on the absolute value of the carrier density and on the carrier temperature. To take this into account, either the coefficient A has to be considered as not constant or the carrier density effective in the second term on the right hand side of Eq. (5) should be taken smaller than n. The coefficient B might also depend on carrier density and temperature.

Moreover, stimulated recombination, not taken into account in Eq. (5), might impose reduction of carrier density at high injection levels. Consequently, even the second order rate equation without the last term in Eq. (5) describing the Auger processes could possibly be sufficient to describe the carrier dynamics, provided that the nonlinearities of coefficients A and B are properly taken into account.

The most straightforward means to avoid the droop effect, whatever its origin, is to increase the chip size and get large emission flux at lower current densities corresponding to high EQE. This approach has been currently exploited to fabricate UV LEDs with the junction area of up to 1 mm^2. CW optical power of 30 and 6 mW was achieved for such LEDs emitting at 273 and 247 nm, respectively [119]. A similar approach to avoid the droop is fabrication of UV LED lamps with multiple micro-pixel device geometry. It is already demonstrated that the output power of up to 40 mW in CW operation mode at room temperature can be achieved at driving current of 1 A in a micropixel LED emitting at 280 nm and having the total junction area of 880 μm^2 [120]. Improvement of external quantum efficiency enabled fabrication of a multichip LED lamp with peak emission at 281 nm providing 20 mW output power at a driving current of 220 mA [121].

4. Conclusions

A currently typical deep UV LED design is depicted in Fig. 15. Up to now, sapphire is the most popular substrate for AlGaN-based deep UV LEDs. Improvement of buffer layers for growing subsequent **c** direction AlGaN layers of a higher structural quality and growing AlGaN layers of nonpolar or semipolar orientations are alternatives that are being currently studied. Deposition of AlGaN layers on bulk AlN substrates is desirable but still needs a breakthrough in growth of high-area bulk AlN substrates at considerably lower costs. HVPE-grown bulk-like AlN substrates, though currently unavailable on a large scale, might be a good solution. The comparatively low external quantum efficiency of deep UV LEDs might be caused by low electron and hole injection, which can be improved by improved doping and better LED design, by still definitely poor internal quantum efficiency of AlGaN MQWs, which can be enhanced by growing

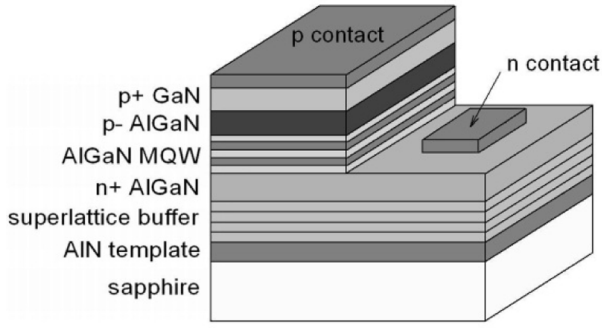

Fig. 15. Currently typical deep UV LED design.

structures with better structural quality, and by low light extraction efficiency, which can be improved by adopting tricks used for InGaN-based LEDs, first of all, by using a flip-chip configuration. To possibly diminish the efficiency droop effect, origin of this effect has to be revealed. Concurrent influence of several mechanisms leading to this effect is rather probable.

References

[1] X. Hu, J. Deng, J.P. Zhang, A. Lunev, Y. Bilenko, T. Katona, M.S. Shur, R. Gaska, M. Shatalov, and A. Khan, Phys. Status Solidi A **203**, 1815 (2006).
[2] S.R. Lee, A.F. Wright, M.H. Crawford, G.A. Petersen, J. Han, and R.M. Biefeld, Appl. Phys. Lett. **74**, 3344 (1999).
[3] D. Korakakis, K.F. Ludwig, Jr., and T.D. Moustakas, Appl. Phys. Lett. **71**, 72 (1997).
[4] P. Ruterana, G. De Saint Jores, M. Laügt, F. Omnes, and E. Bellet-Amalric, Appl. Phys. Lett. **78**, 344 (2001).
[5] E. Iliopoulos, K.F. Ludwig, Jr., T.D. Moustakas, and S.N.G. Chu, Appl. Phys. Lett. **78**, 463 (2001).
[6] M. Benamara, L. Kirste, M. Albrecht, K.W. Benz, and H.P. Strunk, Appl. Phys. Lett. **82**, 547 (2003).
[7] D. Rudloff, T. Riemann, J. Christen, Q.K.K. Liu, A. Kaschner, A. Hoffmann, Ch. Thomsen, K. Vogeler, M. Diesselberg, S. Einfeldt, and D. Hommel, Appl. Phys. Lett. **82**, 367 (2003).
[8] J. Li, K.B. Nam, M.L. Nakarmi, J.Y. Lin, H.X. Jiang, P. Carrier, and S.-H. Wei, Appl. Phys. Lett. **83**, 5163 (2003).
[9] M. Suzuki, T. Uenoyama, and A. Yanase, Phys. Rev. B **52**, 8132 (1995).
[10] S.-H. Wei and A. Zunger, Appl. Phys. Lett. **69**, 2719 (1996).
[11] K.B. Nam, J. Li, M.L. Nakarmi, J.Y. Lin, and H.X. Jiang, Appl. Phys. Lett. **84**, 5264 (2004).

[12] S. Wieczorek, W.W. Chow, S.R. Lee, A.J. Fischer, A.A. Allerman, and M.H. Crawford, Appl. Phys. Lett. **84**, 4899 (2004).
[13] M.S. Shur and R. Gaska, IEEE Trans. Electron Dev. **57**, 12 (2010).
[14] A. Khan, K. Balakrishnan, and T. Katona, Nature Photonics **2**, 77 (2008).
[15] A. Khan, M. Shatalov, H.P. Maruska, H.M. Wang, and E. Kuokstis, Jpn. J. Appl. Phys. **44**, 7191 (2005).
[16] NYC-DEP: Catskill Delaware, Energy and Infrastructure, 2011; http://www.energyandinfrastructure.com/.
[17] "Ultra-violet germicidal mask system", US Patent 5 165 395 Nov. 24, 1992.
[18] M. Shur, R. Gaska, and Y. Bilenko, "Ultraviolet radiation-based media purification", U.S. Patent 20 070 196 235, Aug. 23, 2007.
[19] R. Gaska, Y. Bilenko, and M. Shur, "Organism growth suppression using ultraviolet radiation", U.S. Patent 7 553 456, Jun. 30, 2009.
[20] G.A. Shaw, M.L. Nischan, M.A. Iyengar, S. Kaushik, and M.K. Griffin, Proc. SPIE **4126**, 83 (2003).
[21] J.R. Lakowicz, *Principles of Fluorescence Spectroscopy,* (Kluwer Academic/Plenum, New York, 1999).
[22] N. Ryškevič, S. Juršėnas, P. Vitta, E. Bakienė, R. Gaska, A. Žukauskas, Sensors Actuators B **148**, 371 (2010).
[23] P. Vita, N. Kurilčik, S. Juršėnas, A. Žukauskas, A. Lunev, Y. Bilenko, J. Zhang, X. Hu, J. Deng, T. Katona, and R. Gaska, Appl. Phys. Lett. **87**, 084106 (2005).
[24] P.E. Hockberger, Photochem. Photobiol. **76**, 561 (2002).
[25] A. Menter and C.E. Griffiths, Lancet **370**, 272 (2007).
[26] S. Britz, R. Mirecki, and J. Sulivan, in: *Abstracts of Papers of the American Chemical Society* **241**, Meeting Abstract: 180-AGFD (2011).
[27] L. Liu and J.H. Edgar, Mater. Sci. Eng. R **37,** 61 (2002).
[28] G.A. Slack, J. Phys. Chem. Solids **34**, 321 (1973).
[29] G.A. Slack and T. McNelly, J. Cryst. Growth **42**, 560 (1977).
[30] G.A. Slack and T. McNelly, J. Cryst. Growth **34**, 263 (1976); **42**, 560 (1977).
[31] J.C. Rojo, G.A. Slack, K. Morgan, B. Raghothamachar, M. Dudley, and L.J. Schowalter, J. Cryst. Growth **231**, 317 (2001).
[32] L.J. Schowalter, Y. Shusterman, R. Wang, I. Bhat, G. Arunmozhi, and G.A. Slack, Appl. Phys. Lett. **76**, 985 (2000);
[33] J.C. Rojo, L.J. Schowalter, R. Gaska, M. Shur, M.A. Khan, J. Yang, D.D. Koleske, and J. Cryst. Growth **240**, 508 (2002).
[34] R. Gaska, C. Chen, J. Yang, E. Kuokstis, A. Khan, G. Tamulaitis, I. Yilmaz, M.S. Shur, J.C. Rojo, and L.J. Schowalter, Appl. Phys. Lett. **81**, 4658 (2002).
[35] J.R. Grandusky, S.R. Gibb, M.C. Mendrick, C. Aig Moe, M. Wraback, and L.J. Schowalter, Appl. Phys. Express **4**, 082101 (2011).
[36] V. Adivarahan, Q. Fareed, S. Srivastava, T. Katona, M. Gaevski, M.A. Khan, Jpn. J. Appl. Phys. **46**, L537 (2007).
[37] R. Juza and H. Hahn, Anorg. Allgem. Chem. **224**, 133 (1940).
[38] H.P. Maruska and J.J. Tietjen, Appl. Phys. Lett. **15**, 367 (1969).
[39] H. Amano, M. Kito, K. Hiramatsu, and I. Akasaki, Jpn. J. Appl. Phys. Part 2 **28**, L2112 (1989).
[40] S. Nakamura, Jpn. J. Appl. Phys. Part 2 **30**, L1705 (1991).
[41] A. Bykhovski, B. Gelmont, and M.S. Shur, J. Appl. Phys. **74**, 6734 (1993).
[42] A.D. Bykhovski, B.L. Gelmont, and M.S. Shur, J. Appl. Phys. **81**, 6332 (1997).
[43] A. Usui, H. Sunakawa, A. Sakai, A.A. Yamaguchi, Jpn. J. Appl. Phys. Part 2 **36**, L899 (1999).
[44] P. Fini, J.P. Ibbetson, H. Marchand, B. Moran, L. Zhao, S.P. Denbaars, J.S. Speck, and U.K. Mishra, Mater. Res. Soc. Symp. Proc. **572**, 315 (1999).
[45] R. Jain, W. Sun, J. Yang, M. Shatalov, X. Hu, A. Sattu, A. Lunev, J. Deng, I. Shturm, Y. Bilenko, M. Shur, and R. Gaska, Appl. Phys. Lett. **93**, 051113 (2008).
[46] F.G. McIntosh, K.S. Boutros, J.C. Roberts, S.M. Bedair, E.L. Piner, and N.A. El-Masry, Appl. Phys. Lett. **68**, 40 (1996).
[47] M. Asif Khan, J.W. Yang, G. Simin, R. Gaska, M.S. Shur, H. zur Loye, G. Tamulaitis, A. Zukauskas, D.J. Smith, D. Chandrasekhar, and R. Bicknell-Tassius, Appl. Phys. Lett. **76**, 1161 (2000).
[48] R. Gaska, A.D. Bykhovski, and S. Shur, Appl. Phys. Lett. **73**, 3577 (1998).
[49] M. Asif Khan, J.W. Yang, G. Simin, R. Gaska, M.S. Shur, and A. Bykhovsky, Appl. Phys. Lett. **75**, 2806 (1999).
[50] J. Zhang, E. Kuokstis, Q. Fareed, H. Wang, J. Yang, G. Simin, M. Asif Khan, R. Gaska and M. Shur, Appl. Phys. Lett. **79**, 925 (2001).
[51] G. Tamulaitis, K. Kazlauskas, S. Juršėnas, A. Žukauskas, M.A. Khan, J.W. Yang, J. Zhang, G. Simin, M.S. Shur, and R. Gaska, Appl. Phys. Lett. **77**, 2136 (2000).
[52] R.S. Qhalid Fareed, J.P. Zhang, R. Gaska, G. Tamulaitis, J. Mickevicius, R. Aleksiejunas, M.S. Shur, and M.A. Khan, Phys. Status Solidi C **2**, 2095 (2005).
[53] R. Gaska, J. Zhang, and M. Shur, "Layer growth using metal film and / or islands", US Patent 7 491 626, Feb. 17, 2009.
[54] R. Gaska, J. Zhang, and M.S. Shur, "Nitride-based Light emitting heterostructure", US Patent 7 326 963, Feb. 5, 2008.
[55] R. Gaska, M. Shur, and J. Zhang, "Heterostructure including light generating structure contained in

potential well", US Patent Application 20070181869 (pending).
[56] J. Zhang, X. Hu, A. Lunev, J. Deng, Y. Bilenko, T.M. Katona, M.S. Shur, R. Gaska, and M.A. Khan, Jpn. J. Appl. Phys. Part 1 **44**, 7250 (2005).
[57] R. Gaska, M.S. Shur, and J. Zhang, in: *Proceedings of the Eight International Conference on Solid-State and Integrated Circuit Technology ICSICT-2006*, Shanghai, China, pp. 842–844 [unpublished], 2006.
[58] F. Bernardini and V. Fiorentini, Phys. Rev. B **57**, R9427 (1998).
[59] A. Pinos, S. Marcinkevičius, K. Liu, M.S. Shur, E. Kuokštis, G. Tamulaitis, R. Gaska, J. Yang, and W. Sun, Appl. Phys. Lett. **92**, 061907 (2008).
[60] J. Mickevičius, E. Kuokštis, V. Liuolia, G. Tamulaitis, M. S. Shur, J. Yang, and R. Gaska, Phys. Status Solidi A **207**, 423 (2010).
[61] F. Della Sala, A. Di Carlo, P. Lugli, F. Bernardini, V. Fiorentini, R. Scholz, and J.-M. Jancu, Appl. Phys. Lett. **74**, 2002 (1999).
[62] E. Kuokstis, W.H. Sun, C.Q. Chen, J.W. Yang, and M. Asif Khan, J. Appl. Phys. **97**, 103719 (2005).
[63] P.G. Eliseev, P. Perlin, J. Lee, and M. Osinski, Appl. Phys. Lett. **71**, 569 (1997).
[64] T.Y. Lin, J.C. Fan, and Y.F. Chen, Semicond. Sci. Technol. **14**, 406 (1999).
[65] E. Kuokstis, J.W. Yang, G. Simin, M. Asif Khan, R. Gaska, and M.S. Shur, Appl. Phys. Lett. **80**, 977 (2002).
[66] E. Kuokstis, Jianping Zhang, J.W. Yang, G. Simin, M. Asif Khan, R. Gaska, and M. Shur, Phys. Status Solidi B **228**, 559 (2001).
[67] E. Kuokstis, W.H. Sun, C.Q. Chen, J.W. Yang, and M. Asif Khan, J. Appl. Phys. **97**, 103719 (2005).
[68] K. Balakrishnan, V. Adivarahan, Q. Fareed, M. Lachab, B. Zhang, and A. Khan, Jpn. J. Appl. Phys. **49**, 040206 (2010).
[69] S. Chichibu, K. Wada, and S. Nakamura, Appl. Phys. Lett. **71**, 2346 (1997).
[70] A. Vertikov, A.V. Nurmikko, K. Doverspike, G. Bulman, and J. Edmond, Appl. Phys. Lett. **73**, 493 (1998).
[71] Y. Narukawa, Y. Kawakami, M. Funato, S. Fujita, S. Fujita, and S. Nakamura, Appl. Phys. Lett. **70**, 981 (1997).
[72] Y.S. Lin, K.J. Ma, C. Hsu, S.W. Feng, Y.C. Cheng, C.C. Liao, C. C. Yang, C.C. Chou, C.M. Lee, and J.I. Chyi, Appl. Phys. Lett. **77**, 2988 (2000).
[73] T. Matsuoka, MRS Internet J. Nitride Semicond. Res. **3**, 54 (1998).
[74] Y.P. Varshni, Phys. Status solidi **19**, 459 (1967).
[75] E.L. Ivchenko and A.N. Reznitsky, Phil. Mag. B **65**, 733 (1992).
[76] D. Monroe, Phys. Rev. Lett. **54**, 146 (1985).
[77] R. Zimmermann and E. Runge, Phys. Status Solidi A **164**, 511 (1997).
[78] Yong-Hoon Cho, G.H. Gainer, J.B. Lam, J.J. Song, W. Yang, and W. Jhe, Phys. Rev. B **61**, 7203 (2000).
[79] H.S. Kim, R.A. Mair, J. Li, J.Y. Lin, and H.X. Jiang, Appl. Phys. Lett. **76**, 1252 (2000).
[80] Y.-H. Cho, G.H. Gainer, J B. Lam, J.J. Song, and W. Yang, Phys. Status solidi A **188**, 815 (2001).
[81] C.H. Chen, L.Y. Huang, Y.F. Chen, H.X. Jiang, and J.Y. Lin, Appl. Phys. Lett. **80**, 1397 (2002).
[82] K. Kazlauskas, G. Tamulaitis, A. Žukauskas, M.A. Khan, J.W. Yang J. Zhang, G. Simin, M.S. Shur, and R. Gaska, Phys. Status Solidi C **0**, 512–515 (2002).
[83] K. Kazlauskas, G. Tamulaitis, A. Žukauskas, M.A. Khan, J.W. Yang J. Zhang, E. Kuokstis, G. Simin, M.S. Shur, and R. Gaska, Appl. Phys. Lett. **82**, 4501 (2003).
[84] J. Li, K.B. Nam, J.Y. Lin, and H.X. Jiang, Appl. Phys. Lett. **79**, 3245 (2001).
[85] S.D. Baranovskii, R. Eichmann, and P. Thomas, Phys. Rev. B **58**, 13081 (1998).
[86] M.S. Skolnick, P.R. Tapster, S.J. Bass, A.D. Pitt, N. Apsley, and S.P. Aldred, Semicond. Sci. Technol. **1**, 2896 (1986).
[87] K. Kazlauskas, G. Tamulaitis, A. Zukauskas, M.A. Khan, J.W. Yang, J. Zhang, G. Simin, M.S. Shur, and R. Gaska, Appl. Phys. Lett. **83**, 3722 (2003).
[88] K. Kazlauskas, G. Tamulaitis, P. Pobedinskas, A. Žukauskas, M. Springis, C.-F. Huang, Y.-C. Cheng, and C.C. Yang, Phys. Rev. B **71**, 085306 (2005).
[89] A. Žukauskas, K. Kazlauskas, G. Tamulaitis, M.A. Khan, J.W. Yang, J. Zhang, G. Simin, M.S. Shur, and R. Gaska, Phys. Status solidi C **0**, 2737 (2003).
[90] K. Kazlauskas, A. Žukauskas, G. Tamulaitis, J. Mickevičius, M.S. Shur, R.S. Qhalid Fareed, J.P. Zhang, and R. Gaska, Appl. Phys. Lett. **87**, 172102 (2005).
[91] A. Pinos, V. Liuolia, S. Marcinkevicius, J. Yang, R. Gaska, and M.S. Shur, Appl. Phys. Lett. **109**, 113516 (2011).
[92] Q. Sun, Y. Huang, H. Wang, J. Chen, R.Q. Jin, S.M. Zhang, H. Yang, D.S. Jiang, U. Jahn, and K.H. Ploog, Appl. Phys. Lett. **87**, 121914 (2005).
[93] X.I. Wang, D.G. Zhao, D.S. Jiang, H. Yang, J.W. Liang, U. Jahn, and K. Ploog, J. Phys. Cond. Matter **19**, 176005 (2007).
[94] S. Kim, J. Oh, J. Kang, D. Kim, J. Won, J.W. Kim, and H.-K. Cho, J. Cryst. Growth **262**, 7 (2004).
[95] A. Pinos, S. Marcinkevičius, M. Usman, and A. Hallèn, Appl. Phys. Lett. **95**, 112108 (2009).
[96] G. Tamulaitis, J. Mickevičius, K. Kazlauskas, A. Žukauskas, M.S. Shur, J. Yang, and R. Gaska, Phys. Status Solidi C **8**, 2130 (2011).
[97] S. Watanabe, N. Yamada, M. Nagashima, Y. Ueki, C. Sasaki, Y. Yamada, T. Taguchi, K. Tadatomo, H. Okagawa, and H. Kudo, Appl. Phys. Lett. **83**, 4906 (2003).

[98] M. Shatalov, J. Yang, W. Sun, R. Kennedy, R. Gaska, K. Liu, M. Shur, and G. Tamulaitis, J. Appl. Phys. **105**, 073103 (2009).
[99] R.S. Qhalid Fareed, J.P. Zhang, R. Gaska, G. Tamulaitis, J. Mickevicius, R. Aleksiejunas, M.S. Shur, and M.A. Khan, Phys. Status Solidi C 2, 2095 (2005).
[100] R. Gaska, J. Zhang, and M. Shur, "Layer Growth Using Metal Film and / or Islands", United States Patent Application 20060286782 (2006).
[101] R.G. Banal, M. Funato, and Y. Kawakami, Appl. Phys. Lett. 99, 011902 (2011).
[102] A. Bhattacharyya, T.D. Moustakas, L. Zhou, D.J. Smith, and W. Hug, Appl. Phys. Lett. **94**, 181907 (2009).
[103] T. Mukai, M. Yamada, and S. Nakamura, Jpn. J. Appl. Phys. **38**, 3976 (1999).
[104] S. Watanabe, N. Yamada, M. Nagashima, Y. Ueki, C. Sasaki, Y. Yamada, T. Taguchi, K. Tadatomo, H. Okagawa, and H. Kudo, Appl. Phys. Lett. **83**, 4906 (2003).
[105] Y.-L. Li, Y.-R. Huang, and Y.-H. Lai, Appl. Phys. Lett. **91**, 181113 (2007).
[106] W. Sun, M. Shatalov, J. Deng, X. Hu, J. Yang, A. Lunev, Y. Bilenko, M. Shur, and R. Gaska, Appl. Phys. Lett. **96**, 061102 (2010).
[107] M.F. Schubert and J.K. Kim, Int. High Speed Electron. Syst. **20**, 247 (2011).
[108] I.V. Rozhansky and D.A. Zakheim, Phys. Status Solidi C **3**, 2160 (2006).
[109] M.-H. Kim, M.F. Schubert, Q. Dai, J.K. Kim, E.F. Schubert, J. Piprek, and Y. Park, Appl. Phys. Lett. **91**, 183507 (2007).
[110] M.F. Schubert, S. Chhajed, J.K. Kim, E.F. Schubert, D.D. Koleske, M.H. Crawford, S.R. Lee, A.J. Fischer, G. Thaler, M.A. Banas, Appl. Phys. Lett. **91**, 231114 (2007).
[111] I.A. Pope, P.M. Smowton, P. Blood, J.D. Thompson, M. J. Kappers, and C.J. Humpreys, Appl. Phys. Lett. **82**, 2755 (2003).
[112] A.A. Efremov, N.I. Bochkareva, R.I. Gorbunov, D.A. Larinovich, Y.T. Rebane, D.V. Tarkhin, and Y.G. Shreter, Semiconductors **40**, 605 (2006).
[113] B. Monemar and B.E. Sernelius, Appl. Phys. Lett. **91**, 181103 (2007).
[114] Y.C. Shen, G.O. Mueller, S. Watanabe, N.F. Gardner, A. Munkholm, and M.R. Krames, Appl. Phys. Lett. **91**, 141101 (2007).
[115] N.F. Gardner, G.O. Mueller, Y.C. Shen, G. Chen, S. Watanabe, W. Gotz, and M.R. Krames, Appl. Phys. Lett. **91**, 243506 (2007).
[116] A. Haug, J. Phys. C Solid State Phys. **16**, 4159 (1983).
[117] K.T. Delaney, P. Rinke, and C.G. Van de Walle, Appl. Phys. Lett. **94**, 191109 (2009).
[118] E. Kioupakis, P. Rinke, K.T. Delaney, and C.G. Van de Walle, Appl. Phys. Lett. **98**, 161107 (2011).
[119] M. Shatalov, W. Sun, Y. Bilenko, A. Sattu, X. Hu, J. Deng, J. Yang, M. Shur, C. Moe, M. Wraback, and R. Gaska, Appl. Phys. Express **3**, 062101 (2010).
[120] V. Adivarahan, A. Heidari, B. Zhang, Q. Fareed, S. Hwang, M. Islam, and A. Khan, Appl. Phys Express **2**, 102101 (2009).
[121] S. Hwang, M. Islam, B. Zhang, M. Lachab, J. Dion, A. Heidari, H. Nazir, V. Adivarahan, and A. Khan, Appl. Phys. Express **4**, 012102 (2011).

ULTRAVIOLETINIAI ŠVIESTUKAI

G. Tamulaitis

Vilniaus universiteto Puslaidininkių fizikos katedra ir Taikomųjų mokslų institutas, Vilnius, Lietuva

Santrauka

Straipsnyje apžvelgta pažanga kuriant gilaus ultravioleto šviesos diodus su aktyviąja terpe iš trečiosios grupės elementų nitridinių junginių. Supažindinama su svarbiausiomis gilaus ultravioleto šviesos diodų prietaikomis. Medžiagos savybių apžvalgoje daugiausia dėmesio skiriama gardelės konstantų neatitikimui tarp padėklo ir aktyviosios terpės bei aktyvųjį sluoksnį sudarančių daugialypių kvantinių šulinių heterosandūrose, nepusiausvirųjų kvazidalelių lokalizacijai, medžiagų savybėms, ribojančioms vidinį kvantinį našumą, ir našumo smukimui esant dideliam nepusiausvirųjų krūvininkų tankiui. Gilaus ultravioleto šviesos diodų gamybai šiuo metu daugiausia naudojamas AlGaN, todėl apžvalgoje plačiausiai aptarinėjamos šio junginio savybės. Straipsnyje pateikiama informacijos ir apie giminingą plačiatarpį keturgubą junginį AlInGaN.